SUPPLEMENTARY MATERIAL

Transport of bacterial cell (*E.coli*) from different recharge water resources in porous media during simulated artificial groundwater recharge

Wei Fan, Qi Li, Mingxin Huo, Xiaoyu Wang, Shanshan Lin (✉)

School of Environment, Northeast Normal University, 2555 Jingyue St., Changchun, 130117, China.

Corresponding author **(✉)**

Shanshan Lin

E-mail address: linpapersubmit@163.com (Shanshan Lin)

Tel. : +86-431-89165610;

Fax. : +86-431-89165621.

S1 analyses of the 3DEEM spectra

The fluorescence spectra were divided into five regions, representing five corresponding DOM types based upon their excitation-emission properties (Chen et al., 2003). Rayleigh scattering was removed by subtracting the blank spectrum and Raman scattering was adjusted by interpolation, followed by fluorescence regional integration (FRI) to calculate the percentage fluorescence response (P_i, %) for quantitative analysis of fluorescence EEMs (Chen et al., 2003). As shown in Fig. 1, the distribution of fluorescence intensity varied notably across the three types of recharge water assessed. The DOM in SE had fluorophores in region III with a respective EEM center and exhibited EEM shoulders in regions IV and V, with a similar distribution observed for river water, although fluorophores were in regions II and III. In contrast, the fluorophores in rainfall water were distributed in regions I and II, with the possibility that the DOC was too low to effectively identify its fluorescence properties. In rainfall water, the relative contributions of P to DOM were 42.26% and 33.05%, in region I (tyrosine-like substances) and region II (tryptophan-like substances) respectively, followed by region III (fulvic acid-like substances) with 10.99%, region IV (soluble microbial by-product) with 8.69% and region V (humic acid-like organics) with 5.01%. For river water, the distribution of contribution of P in the five DOM fractions, were relatively uniform and varied in the range of 13.72-25.74%. SE is rich in fulvic acid-like substances (P_{III}=28.08%) and soluble microbial metabolites (P_{IV}=24.48%) as stated in the literature (Hao et al., 2012), and the proportion of P in DOM regions I, II and V was 6.47%, 21.55% and 19.42%, respectively. When *E. coli* cells dwell and grow in recharge ponds containing recharge water, the different physiological responses observed are likely to be induced by the different levels of nutrient deprivation in different recharge water resources.

S2 the outer membrane proteins (OMPs) assay

The OMPs of the *E. coli* cells were extracted and profiled using sodium dodecyl-sulfate polyacrylamide gel electrophoresis (SDS-PAGE) as described by Laemmli (1970). Cell samples cultivated in LB for 16 h, and cells that were then starved in SE, river water and rainfall for 50 h were taken to examine, and the cultures were adjusted to the same optical density OD_{600} of 0.5. Briefly, E. coli cells were harvested by centrifugation (10,000×g/4 ℃, 10 min), then resuspended in 5 mL sterile NaCl (0.15 M). The supernatant was centrifuged again at 10,000 × g for 10 min at 4 ℃ to pellet the membranes. To solubilise the OMPs, the membranes were resuspended in 2% sodium lauryl sarcosinate (Sigma) at room temperature for 1 h. Centrifugation at 100,000 × g (40 min, 4 ℃) was performed again to pellet the OMPs. The resulting OMP pellet was resuspended in 0.25 mL sterile 0.15 M NaCl solution, the OMPs were separated on 12% SDS gel by SDS-PAGE and stained by Brilliant Blue G-Colloidal Concentrate 2025 (Sigma) (Chourabi et al., 2017). The concentration of OMPs in the final preparation was determined using the Bradford assay (Thermo Scientific, NanoDrop 2000).

S3 the interaction energy calculation using XDLVO theory

The E.coli cells-sand particles interaction energy under selected solution chemistry conditions were examined using Extended Derjaguin Landau Verwey Overbeek (XDLVO) theory. This theory considers the total interaction energy of cell-sand as the sum of the Lifshitz-van der Waals (LW), the electrostatic double layer (EDL), and the Lewis acid-base (AB) interactions. The interaction energy (∅) can be calculated as (Li et al., 2018; Yan et al., 2019):

$$\emptyset^{Total}=\emptyset^{VDW}+\emptyset^{EDL}+\emptyset^{AB} \quad (S1)$$

$$\Delta G^{LW}=-\frac{Ar}{6h}\left(1+\frac{14h}{\lambda}\right)^{-1} \quad (S2)$$

$$\Delta G^{EDL}=\pi r\varepsilon\varepsilon_0\left\{2\zeta_b\zeta_s\ln\left[\frac{1+\exp(-\kappa h)}{1-\exp(-\kappa h)}\right]+(\zeta_b^2+\zeta_s^2)\ln[1-\exp(-2\kappa h)]\right\} \quad (S3)$$

$$\Delta G^{AB}=2\pi r\lambda_{AB}\Delta G_{h_0}^{AB}\exp\left(\frac{h_0-h}{\lambda_{AB}}\right) \quad (S4)$$

Where A is the Hamaker constant, h is the separation distance, r is the radius of the bacterial cell, λ is the characteristic of the wavelength (100 nm), ε_0 is the dielectric permittivity of vacuum (8.854×10^{-12} C/V m), ε is the dielectric constant of water (78.55), ζ is the surface potential, the subscripts b and s denote as bacteria and sand, κ^{-1} is the Debye-Hückel reciprocal length, λ_{AB} is the characteristic decay length of AB interactions in water (0.6 nm), h_0 is the distance of the closest approach, $\Delta G_{h_0}^{AB}$ is the AB interaction free energy per unit area corresponding to h_0.

$$A=24\pi h_0^2\left(\sqrt{\gamma_b^{LW}}-\sqrt{\gamma_w^{LW}}\right)\left(\sqrt{\gamma_s^{LW}}-\sqrt{\gamma_w^{LW}}\right) \quad (S5)$$

$$\kappa=\sqrt{\frac{2N_A e^2 I}{\varepsilon_r\varepsilon_0 K_B T}} \quad (S6)$$

$$\Delta G_{h_0}^{AB}=2\left[\sqrt{\gamma_w^+}\left(\sqrt{\gamma_b^-}+\sqrt{\gamma_s^-}-\sqrt{\gamma_w^-}\right)+\sqrt{\gamma_w^-}\left(\sqrt{\gamma_b^+}+\sqrt{\gamma_s^+}-\sqrt{\gamma_w^+}\right)-\sqrt{\gamma_b^-\gamma_s^+}-\sqrt{\gamma_b^+\gamma_s^-}\right] \quad (S7)$$

Where, N_A is the Avogadro constant (6.02×10^{23} /mol); *e* is the elementary charge (1.602×10^{-19} C); *I* is the ionic strength, K_B is the Boltzmanm constant (1.381×10^{-23} J/K); *T* is the absolute temperature (294.50 K). The subscripts of *b*, *s*, and w represent bacteria cells, sand and water, respectively. For quartz sands, the reported values of γ_s^{LW}, γ_s^+ and γ_s^- are 39.2, 1.4, and 47.8 mJ/m^2, and they were 21.8, 25.5, and 25.5 for water phase correspondingly (Li et al., 2018; Yan et al., 2019).

The γ^{LW} values of the *E.coli* cells can be calculated from the electron-accepting and electron-donating interfacial tension values, the surface interfacial tension parameters of the selected probing liquids (γ_i^L), and contact angles (θ) of cells in three probing liquids (water, glycerol, and diiodomethane):

$$\gamma_i^L(1+\cos\theta) = 2\sqrt{\gamma_i^{LW}\gamma^{LW}} + 2\sqrt{\gamma_i^+\gamma^-} + 2\sqrt{\gamma_i^-\gamma^+} \quad \text{(S8)}$$

Where the subscript *i* represents water (γ^L=72.8, γ^{LW}=21.8, γ^+=γ^-=25.5 mJ/m^2), glycerol (γ^L=64.0, γ^{LW}=34.0, γ^+=3.92, γ^-=57.4 mJ/m^2), and diiodomethane (γ^L=50.8, γ^{LW}=50.8, γ^+=γ^-=0 mJ/m^2), respectively.

S4 numerical modelling

One dimensional advection-dispersion equations were used to describe the transport process of *E. coli* cells in the saturated sand columns, as defined in Equations (S9)-(S10) (Fan et al., 2015; Chu et al., 2019):

$$\frac{\partial(nC)}{\partial t} + \rho\frac{\partial S}{\partial t} = nD\frac{\partial^2 C}{\partial x^2} - q\frac{\partial C}{\partial x} \quad \text{(S9)}$$

$$\rho\frac{\partial S}{\partial t} = nk_{att}\psi C - k_{det}\rho S \quad \text{(S10)}$$

$$\psi = \left(1-\frac{S}{S_{\max}}\right)\left(\frac{d_c+x}{d_c}\right)^{-\beta} \quad \text{(S11)}$$

Where, n is the porosity; C is the concentration of cells in liquid phase; ρ is the bulk density of the packed sand; S is the concentration of cells in the porous medium; q is the flow rate; k_{att} and k_{det} are the attachment and detachment coefficients; ψ is a dimensionless deposition function for *E. coli* cells; $S_{\max}$ is the maximum concentration of deposited *E. coli* cells; d_c is the average sand diameter and β is an empirical variable (with an optimal value of 0.432 suggested by Bradford et al. (2003)). This model can describe multiple mechanisms of cells transport, including advection, dispersion, straining, blocking and attachment/detachment (Zhou et al., 2016). The model was inversely fitted to data from the BTCs, to determine the parameters k_{att}, k_{det} and $S_{\max}$. The conventional attachment and detachment model, without considering the blocking and straining effects, was obtained by setting $\psi = 1$.

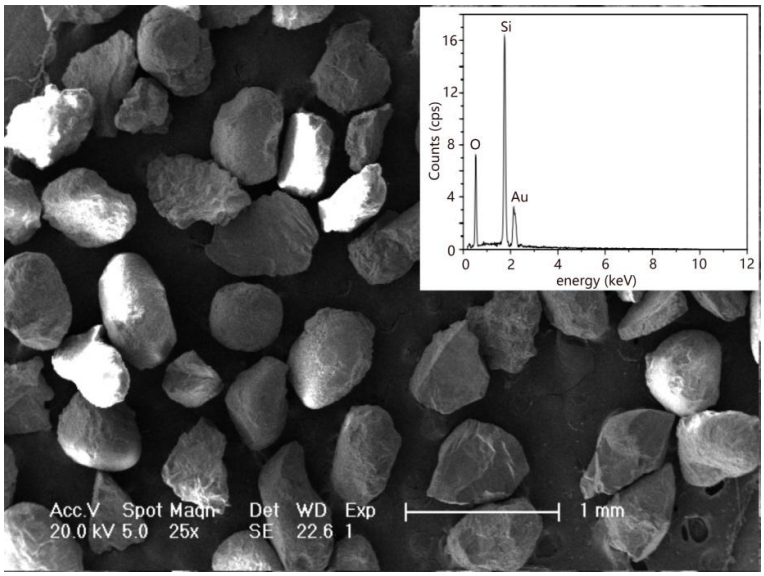

84

85 **Fig. S1** SEM micrographs and EDS patterns of sand grains

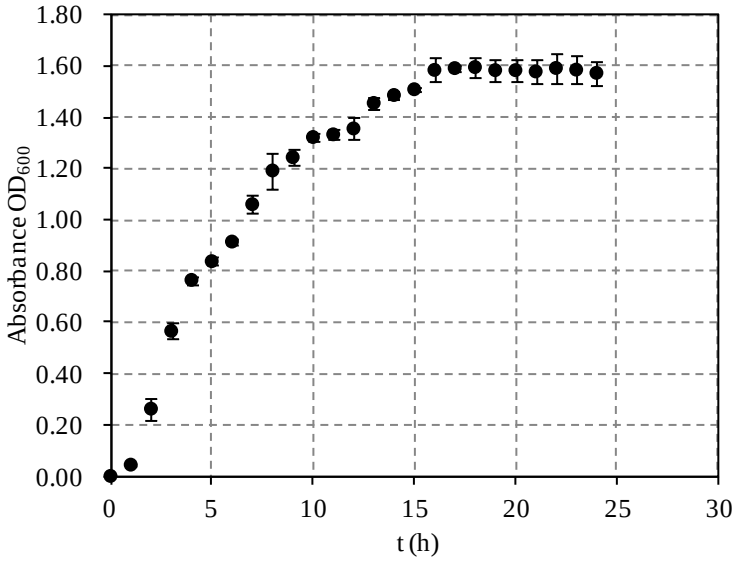

86

87 **Fig. S2** The growth curve of *E.coli*

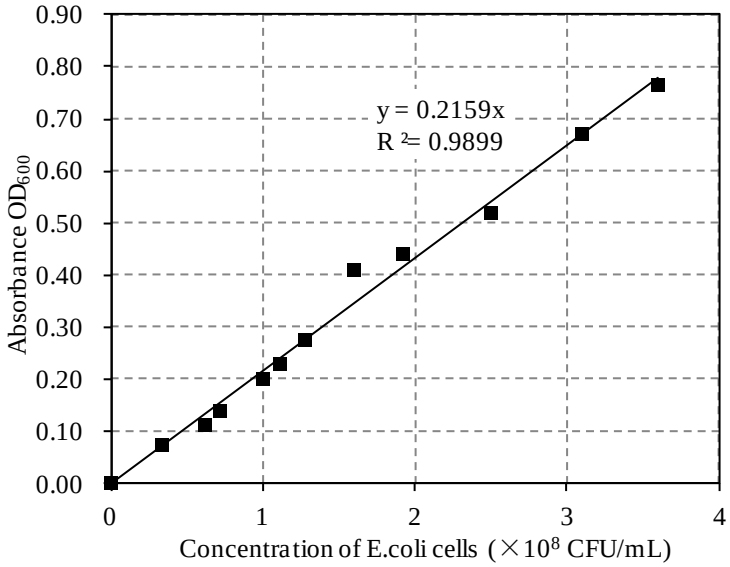

Fig. S3 Standard curve of OD_{600} and the concentration of *E. coli* cells

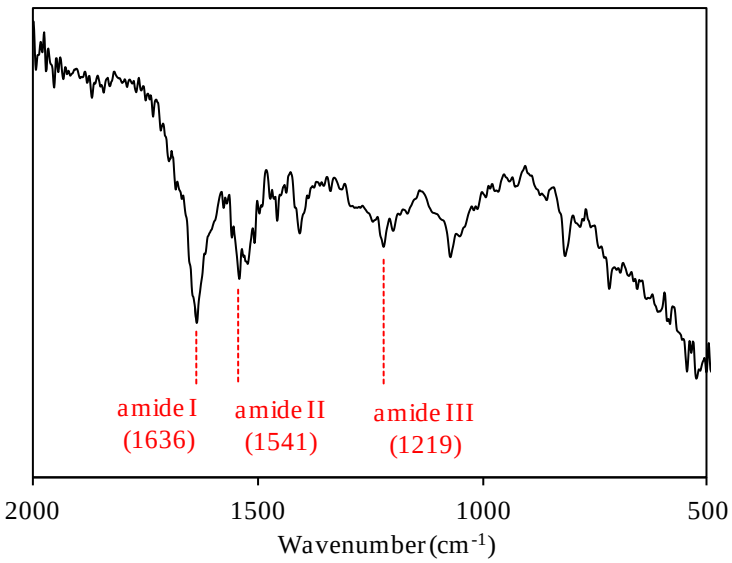

Fig. S4 FTIR spectra of *E. coli* cells

References

Bradford S A, Simunek J, Bettahar M, Van Genuchten M T, Yates S R (2003). Modeling colloid attachment, straining, and exclusion in saturated porous media. Environmental Science & Technology, 37: 2242-2250. doi: 101021/es025899u

Chen W, Westerhoff P, Leenheer J A, Booksh K (2003). Fluorescence excitation-emission matrix regional integration to quantify spectra for dissolved organic matter. Environmental Science & Technology, 37: 5701-5710. doi: 101021/es034354c

Chourabi K, Torrella F, Kloula S, Rodriguez J A, Trabelsi I, Campoy S, Landoulsi A, Chatti A (2017). Adaptation of Shigella flexneri to starvation: morphology, outer membrane proteins and lipopolysaccharide changes. Arabian Journal of Geosciences, 10: 274-280. doi: 101007/s12517-017-3064-3

Chu T, Yang Y S, Lu Y, Du X Q, Ye X Y (2019). Clogging process by suspended solids during groundwater artificial recharge: Evidence from lab simulations and numerical modelling. Hydrological Processes, doi: 101002/hyp13553

Fan W, Jiang X H, Yang W, Geng Z, Huo M X, Liu Z M, Zhou H (2015). Transport of graphene oxide in saturated porous media: Effect of cation composition in mixed Na-Ca electrolyte systems. Science of The Total Environment, 511: 509-515. doi: 101016/jscitotenv201412099

Hao R, Ren H, Li J, Ma Z, Wan H, Zheng X, Cheng S (2012). Use of three-dimensional excitation and emission matrix fluorescence spectroscopy for predicting the disinfection by-product formation potential of reclaimed water. Water Research, 46: 5765-5776. doi: 101016/jwatres201208007

Laemmli U K (1970). Cleavage of structural proteins during the assembly of the head of bacteriophage T4. Nature, 227: 680-685. doi: 10.1038/227680a0.

Li Q, Yang J, Fan W, Zhou D, Wang X, Zhang L, Huo M, Crittenden J C (2018). Different transport behaviors of Bacillus subtilis cells and spores in saturated porous media: Implications for contamination risks associated with bacterial sporulation in aquifer. Colloids and surfaces B: Biointerfaces, 162: 35-42. doi: 101016/jcolsurfb201711018

115 Yan C, Chen T, Shang J (2019). Effect of bovine serum albumin on stability and transport of kaolinite colloid. Water Research, 155:

116 204-213. doi: 101016/jwatres201902022

117 Zhou D D, Jiang X H, Lu Y, Fan W, Huo M X, Crittenden J C (2016). Cotransport of graphene oxide and Cu (II) through saturated

118 porous media. Science of the Total Environment, 550: 717-726. doi: 101016/jscitotenv201601141